

ORIGINAL ARTICLE

Ruthenium nanocrystal decorated vertical graphene nanosheets@Ni foam as highly efficient cathode catalysts for lithium-oxygen batteries

Dawei Su¹, Dong Han Seo², Yuhang Ju³, ZhaoJun Han², Kostya Ostrikov⁴, Shixue Dou⁵, Hyo-Jun Ahn⁶, Zhangquan Peng³ and Guoxiu Wang¹

The electrochemical performance of lithium-oxygen (Li-O₂) batteries can be markedly improved through designing the architecture of cathode electrodes with sufficient spaces to facilitate the diffusion of oxygen and accommodate the discharge products, and optimizing the cathode catalyst to promote the oxygen reduction reaction and oxygen evolution reaction (OER). Herein, we report the synthesis of ruthenium (Ru) nanocrystal-decorated vertically aligned graphene nanosheets (VGNS) grown on nickel (Ni) foam. As an effective binder-free cathode catalyst for Li-O₂ batteries, the Ru-decorated VGNS@Ni foam can significantly reduce the charge overpotential via the effects on the OER and achieve high specific capacity, leading to an enhanced electrochemical performance. The Ru-decorated VGNS@Ni foam electrode has demonstrated low charge overpotential of ~0.45 V and high reversible capacity of 23 864 mAh g⁻¹ at the current density of 200 mA g⁻¹, which can be maintained for 50 cycles under full charge and discharge testing condition in the voltage range of 2.0–4.2 V. Furthermore, Ru nanocrystal decorated VGNS@Ni foam can be cycled for more than 200 cycles with a low overpotential of 0.23 V under the capacity curtailed to be 1000 mAh g⁻¹ at a current density of 200 mA g⁻¹. Ru-decorated VGNS@Ni foam electrodes have also achieved excellent high rate and long cyclability performance. This superior electrochemical performance should be ascribed to the unique three-dimensional porous nanoarchitecture of the VGNS@Ni foam electrodes, which provide sufficient pores for the diffusion of oxygen and storage of the discharge product (Li₂O₂), and the effective catalytic effect of Ru nanocrystals on the OER, respectively. *Ex situ* field emission scanning electron microscopy, X-ray diffraction, Raman and Fourier transform infrared measurements revealed that Ru-decorated VGNS@Ni foam can effectively decompose the discharge product Li₂O₂, facilitate the OER and lead to a high round-trip efficiency. Therefore, Ru-decorated VGNS@Ni foam is a promising cathode catalyst for rechargeable Li-O₂ batteries with low charge overpotential, long cycle life and high specific capacity.

NPG Asia Materials (2016) 8, e286; doi:10.1038/am.2016.91; published online 8 July 2016

INTRODUCTION

Rechargeable Li-O₂ batteries have been considered to be one of the most promising systems as future power sources for electric vehicles owing to their high theoretical energy density of 3505 Wh kg⁻¹.^{1–4} However, the development of practical Li-O₂ batteries faces several serious challenges, including high overpotential between charge and discharge, poor cycling stability, low Coulombic efficiency and low rate capability.^{5–8} The reaction mechanism in a Li-O₂ cell involves an oxygen reduction reaction (ORR) in the discharge process and an oxygen evolution reaction (OER) in the charge process, during which molecular O₂ reacts reversibly with Li⁺ ions (Li⁺+O₂+2e⁻ ↔ Li₂O₂,

with an equilibrium voltage of 2.96 V vs Li).^{9,10} This mechanism is very different from the traditional intercalation reactions of Li-ion batteries. Although the theoretical overpotential for a Li₂O₂ film is only 0.2 V, the practical overpotential normally reaches as high as 1.5 V, because there are limitations on charge transport through the insulating Li₂O₂ particles to the Li₂O₂-electrolyte interface.^{9,11} Therefore, it is essential to lower the charge potential to improve Li-O₂ battery performance. So far, it has been identified that catalysts and appropriate non-aqueous electrolytes can effectively overcome these problems.^{6,7,12} Various catalysts, such as metal oxides, metal nitrides and noble metals have been investigated as suitable cathode catalysts in

¹Centre for Clean Energy Technology, Faculty of Science, University of Technology Sydney, Sydney, NSW, Australia; ²Commonwealth Scientific and Industrial Research Organisation, Lindfield, NSW, Australia; ³State Key Laboratory of Electroanalytical Chemistry, Changchun Institute of Applied Chemistry, Chinese Academy of Science, Yinghua Rd, Chaoyang, Changchun, Jilin, China; ⁴Institute for Future Environments and School of Chemistry, Physics and Mechanical Engineering, Queensland University of Technology, Brisbane, QLD, Australia; ⁵Institute for Superconducting and Electronic Materials, University of Wollongong, Wollongong, NSW, Australia and ⁶School of Materials Science and Engineering, Gyeongsang National University, Jinju-si, Gyeongsangnam-do, Korea
Correspondence: Professor Z Peng, State Key Laboratory of Electroanalytical Chemistry, Changchun Institute of Applied Chemistry, Chinese Academy of Science, Yinghua Rd, Chaoyang, Changchun, Jilin 130022, China.

E-mail: zqpeng@ciac.jl.cn

or Professor G Wang, Centre for Clean Energy Technology, Faculty of Science, University of Technology Sydney, 15 Broadway, Sydney, NSW 2007, Australia.

E-mail: Guoxiu.Wang@uts.edu.au

Received 20 September 2015; revised 11 April 2016; accepted 6 May 2016

Li-O₂ cells to reduce the charge overpotential.^{13–15} The use of catalysts can decrease the charge potential to ~3.8 V from ~4.2 V.^{9,16,17} Therefore, finding suitable cathode catalysts is an effective approach to solve the overpotential problem.^{18–20} Recently, ruthenium (Ru) and RuO₂ have been reported as active catalysts towards the OER, which achieved high reversible capacity, low charge overpotential and good cycling stability.^{21–23}

Because the discharge product Li₂O₂ cannot be dissolved in organic electrolyte, the Li₂O₂ could block the oxygen diffusion path and also could cause volume expansion of the electrode, resulting in electrode degradation. Therefore, optimizing the structure of the cathode materials is crucial to improve the performance of Li-O₂ batteries. Recently, vertical graphene nanosheets (VGNS) showed great promise as electrode materials because of their excellent electrical conductivity, large surface area and, in particular, their inherent three-dimensional (3D) open network structure, with graphene flakes oriented perpendicularly to the electrode surface, in contrast to the usual horizontal graphene.²⁴

Herein, we have developed a one-step, low-cost and environmentally benign natural precursor (butter) approach to the synthesis of VGNS on Ni foam using a plasma-assisted chemical vapor deposition process in a low temperature environment (400 °C) without any non-conductive polymeric binders. We also loaded Ru nanocrystals on the VGNS@Ni foam. The as-prepared Ru-decorated VGNS@Ni foam shows a 3D, open network architecture with the tailored, vertically oriented graphene covering the Ni foam skeleton and forming a channel structure. The Ru nanocrystals are homogeneously distributed on graphene nanosheets. The as-prepared Ru-decorated VGNS@Ni foam can provide sufficient voids to accommodate Li₂O₂ and facilitate oxygen diffusion through the 3D network. It has been proved that this architecture is an important factor that influences the overall electrochemical performance of the Li-O₂ batteries. Furthermore, it can also efficiently reduce the charge overpotential and increase the cycling stability.

EXPERIMENTAL PROCEDURE

Synthesis of VGNS@Ni foam

The deposition of VGNS was carried out in a plasma chemical vapor deposition system. Porous Ni foam was used as the substrate without any catalyst. The Ni foam was firstly pasted with butter before being loaded in the reactor. Care was taken to make sure that the butter remained uniform across a large area. Then, the Ni foam was loaded directly into the radiofrequency inductively coupled plasma chamber. A gas mixture of Ar and H₂ was then fed into the system for growing the VGNS. The power of the radiofrequency plasma was 1000 W, and the growth lasted for 9 min. No external substrate heating was used during the growth process, yet the substrate temperature was estimated to be 400 °C owing to the plasma-heating effects. The H₂ concentration was maintained at 80%, which provided the best graphitic quality for the VGNS. The pressure was maintained at 2.5 Pa throughout the process. The obtained VGNS can reach up to ~0.4 mg cm⁻¹ at the Ni foam skeleton.

Synthesis of Ru@VGNS@Ni foam catalysts

In a typical synthesis process, VGNS@Ni foam materials were dispersed in RuCl₃ solution with constant stirring at room temperature, and then the triblock copolymer (HO(CH₂CH₂O)₁₀₆(CH₂CH(CH₃)-O)₇₀(CH₂CH₂O)₁₀₆H) (Pluronic F127) was added under vigorous stirring for 24 h. After that, the VGNS@Ni foam materials were separated by filtration and dried at room temperature. The dried sample was aged in air at 50 °C for 48 h in a Petri dish and then calcinated by heat treatment at 300 °C for 3 h under 5% H₂/Ar atmosphere.

Structural and physical characterization

The crystal structures and phases of the materials were characterized by X-ray diffraction (XRD; Siemens D5000, Aubrey, TX, USA) using Cu K α radiation. The morphology was analyzed by field emission scanning electron microscopy (FESEM; Zeiss Supra 55VP, Jena, Germany). The details of the structure were further characterized by transmission electron microscopy (TEM) and high-resolution TEM (HRTEM; JEOL JEM-2011, Tokyo, Japan). Selected area electron diffraction patterns were recorded by a Gatan charge-coupled device camera in a digital format. Atom-resolved HRTEM images were obtained by high-angle annular dark field scanning TEM (JEOL JEM-ARM200F, Tokyo, Japan). Optical images were collected with a Canon EOS 660D camera (Tokyo, Japan). Raman spectra were collected using a Renishaw inVia Raman spectrometer system (Renishaw, Gloucestershire, UK) equipped with a Leica DM LB microscope (Leica, Wetzlar, Germany) and a 17 mW at 633 nm Renishaw helium neon laser source. Fourier transform infrared spectra were collected on a Nicolet Magna 6700 FT-IR spectrometer (Thermo Fisher, Scoresby, VIC, Australia) with 0.9 cm⁻¹ standard optical resolution using a KBr beam splitter. Thermogravimetric/differential thermal analysis was performed at a heating rate of 5 °C min⁻¹ under air flow from room temperature to 900 °C on a 2960 SDT system (New Castle, DE, USA), and the Ru-decorated VGNS was measured after being stripped from the Ni skeleton. N₂ adsorption-desorption isotherms were collected on a Micromeritics 3Flex analyzer (Micromeritics Instrument Corporation, Norcross, GA, USA) at the testing temperature of 77 K. Brunauer-Emmett-Teller analysis was used to determine the surface area and was calculated using the isothermal points at a relative pressure of $P/P_0 = 0.05–0.25$.

Electrochemical testing

Swagelok-type cells were designed to investigate the charge and discharge properties and the cyclability in Li-O₂ batteries. The cells consist of a stainless steel cylinder plunger to support a Li foil anode (3 mm \times ϕ 15 mm) and a special stainless steel tube to allow oxygen access to the back side of the cathode. The cathode electrodes were cut into disks with a diameter of 14 mm. Therefore, the active materials of VGNS and Ru-decorated VGNS can reach up to 0.56 and 0.93 mg, respectively. The cathode was placed on the separator, and a thin open disk of 316 stainless steel mesh was placed on top to act as the current collector. The entire cell was gas-tight except for the stainless steel mesh window, which exposed the porous cathode to the O₂ atmosphere. The Li-O₂ cells were assembled in an Ar-filled glove box (Unilab; MBRAUN, Garching, Germany) with water and oxygen levels <0.1 p.p.m. A glass microfiber filter (Whatman, ϕ 21 mm, Maidstone, UK) separator was used, soaked in an electrolyte consisting of 1 M LiNO₃ (99.99%; Sigma-Aldrich, Castle Hill, NSW, Australia) in dimethyl sulfoxide (anhydrous, >99.9%; Sigma-Aldrich). The water content of the electrolyte was measured by a Mettler Toledo C20 Karl Fischer Titrator (Columbus, OH, USA). All measurements were conducted in 1 atm dry oxygen atmosphere to avoid any negative effects of humidity and CO₂. Galvanostatic discharge-charge cycling was conducted on a Neware battery testing system. The specific capacity was calculated according to the mass of the VGNS or Ru-decorated VGNS only. For the electrochemical performance testing, more than 10 cells were tested at each current density. To investigate the charge and discharge products and the corresponding structural and morphological changes, the cells were charged and discharged to the required voltages, and then opened in the glove box. The active materials were removed from the electrodes and washed with dimethyl sulfoxide before being used for *ex situ* XRD, s.e.m., Raman and Fourier transform infrared investigations. The *in situ* differential electrochemical mass spectrometry (DEMS) analyses have been conducted to confirm that the discharge-charge processes were overwhelmingly dominated by ORR/OER in Ru-decorated VGNS@Ni foam Li-O₂ cell. The system is based on a commercial quadrupole mass spectrometer (Thermo Fischer, Waltham, MA, USA) with turbo molecular pump (Pfeiffer Vacuum, Wetzlar, Germany), which is backed by a dry scroll pump (Edwards, Narellan, NSW, Australia), and a leak inlet, which samples from the purge gas stream. For the detection of the gases evolved, Ar carrier gas was used as an internal tracer with a flow rate of 2.0 ml min⁻¹, which was precisely controlled with a digital mass flow controller (Bronkhorst, Ruurlo, Netherlands). Gas chromatography mass spectrometry was performed

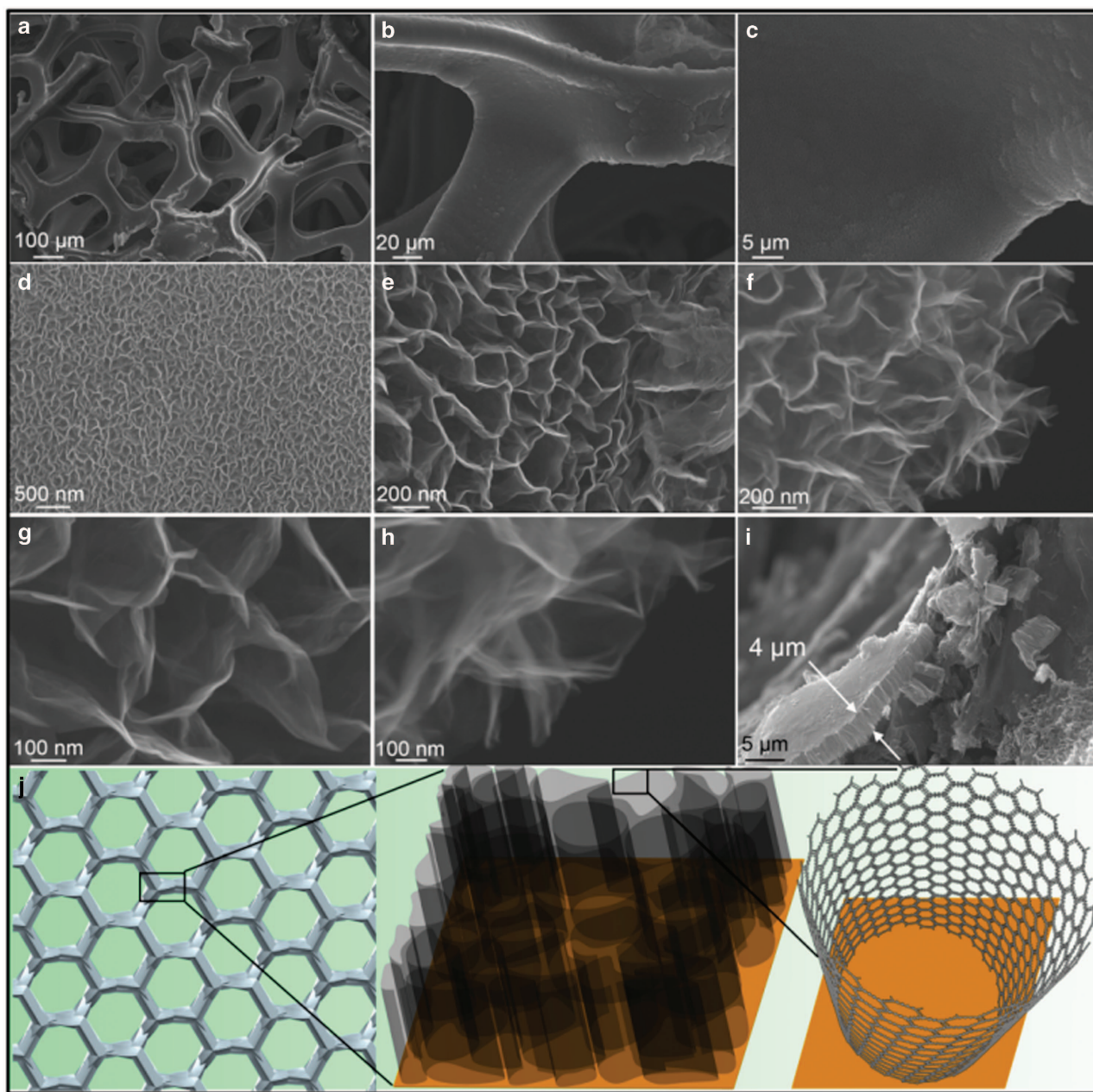


Figure 1 (a–c) Low magnification field emission scanning electron microscopy (FESEM) images of vertical graphene nanosheets (VGNS)@Ni foam. (d–f) High magnification FESEM images of VGNS@Ni foam. (g, h) Highly resolved FESEM images of VGNS@Ni foam. (i) Low magnification cross-sectional FESEM image of VGNS@Ni foam. (j) Schematic illustrations of the VGNS@Ni foam.

using an MD800 benchtop quadrupole mass spectrometer coupled to a GC8000 gas chromatograph (Fisons Instruments, Manchester, UK).

RESULTS AND DISCUSSION

Morphology and crystal structure characterization

The porous Ni foam provides a large volume to accommodate a high density of VGNS and an interconnected conductive network to ensure good electrical conductivity.^{25,26} The VGNS was synthesised from the environmentally benign natural precursor, butter, by a one-step and efficient process because of the unique ability of the plasma. During the whole synthesis process, there is no metal catalyst needed, avoiding the process of removing impurities (catalysts) before device fabrication. In addition, the plasma-assisted chemical vapor deposition

process can synthesize graphene in a lower temperature environment (400 °C) than the conventional chemical vapor deposition method (~1000 °C).²⁷ Figure 1 shows typical FESEM images of VGNS grown on the Ni foam, where the dense and uniform structure of the VGNS was observed, covering the entire Ni foam (Figures 1a–c). Figure 1a clearly demonstrates the 3D porous Ni foam architecture. Binder-free VGNS residing on this highly conductive Ni foam can be seen in Figures 1b and c. There is no cracking, which could expose the Ni skeleton. From the magnified FESEM image (Figures 1d–f), it can be observed that the as-prepared VGNS exhibit strong binding to the Ni foam with a vertical orientation and form a honeycomb structure enclosed by the neighboring VGNS walls. This unique structure also helps avoid the agglomeration of graphene nanosheets that commonly

occurs in wet chemical processing, thus enabling good ion diffusion. Furthermore, the VGNS@Ni possesses good electrical conductivity and a large surface area with minimal tortuosity. The vertical orientation of the as-prepared VGNS is a result of the electric-field-guided growth in the plasma sheath.²⁸ The high-resolution FESEM images (Figures 1g and h) show the high density of edge planes of the as-prepared VGNS. These edge planes are thin enough to be transparent under the low-energy electron beam, indicating their graphene characteristics. The area and thickness of the VGNS can be easily estimated by the amount of butter pasted on the Ni foam. As shown in Figure 1i, the as-prepared VGNS are $\sim 4\ \mu\text{m}$ in thickness. Based to the N_2 adsorption–desorption isotherms measurement, the as-prepared VGNS has the specific Brunauer–Emmett–Teller surface area of $448.2\ \text{m}^2\ \text{g}^{-1}$ (Supplementary Figure S1 and Supplementary Information). In addition, the VGNS shows excellent flexibility, and the structural integrity can be retained after numerous cycles of bending. As illustrated in Figure 1j, the VGNS layer uniformly grew on Ni foam, which is a potential architecture for the storage of the discharge product of Li_2O_2 in Li-O_2 batteries. Furthermore, the 3D porous structure of Ni foam can also facilitate the diffusion of oxygen.

It has been reported that Ru is the most suitable catalyst for the OER and ORR in Li-O_2 batteries.²⁹ Thus, we also used Ru nanocrystals to decorate the VGNS@Ni foam for Li-O_2 battery application. The Ru-nanocrystal-functionalized VGNS@Ni foam was synthesized by an impregnation method. The VGNS@Ni foam was mixed with RuCl_3 solution overnight to accomplish the Ru decoration

and separated by filtration. The typical synthesis process involved the absorption of hydrophilic and hydrophobic triblock copolymer F127. Then, RuCl_3 was added. During this process, Ru ions were absorbed on the long chains of the triblock copolymer through weak coordination bonds between the alkylene oxide segments and the metal ions.³⁰ The final product was obtained by heat treatment in a reducing atmosphere. The Ru content in the Ru-decorated VGNS@Ni foam nanocomposite was determined to be 43 wt%, calculated based on the TGA measurement (Supplementary Figure S2; for the measurement, the Ru-decorated VGNS was stripped from the Ni skeleton). The FESEM images of Ru-decorated VGNS@Ni foam (Figure 2) demonstrated that after deposition of Ru nanocrystals, the 3D porous network of the Ni foam was preserved (Figure 2a). Furthermore, the VGNS was still uniformly coated on the Ni foam skeleton (Figures 2b and c), with about $4\ \mu\text{m}$ thickness (as shown in Figure 2d). The Ru-decorated VGNS@Ni foam nanocomposite also shows the honeycomb architecture (Figure 2e). From the high-resolution FESEM image (Figure 2f), it can be seen that the Ru nanocrystals are coated on both sides of the vertical graphene, forming a sandwich structure. The Ru-decorated graphene still keeps the well-defined robust vertical orientation. Figure 2g shows the horizontal image of the Ru-decorated VGNS@Ni foam nanocomposite, which clearly demonstrates that the Ru nanocrystals are homogeneously distributed along the whole vertical graphene wall. This unique porous nanoarchitecture is further illustrated in Figures 2h and i.

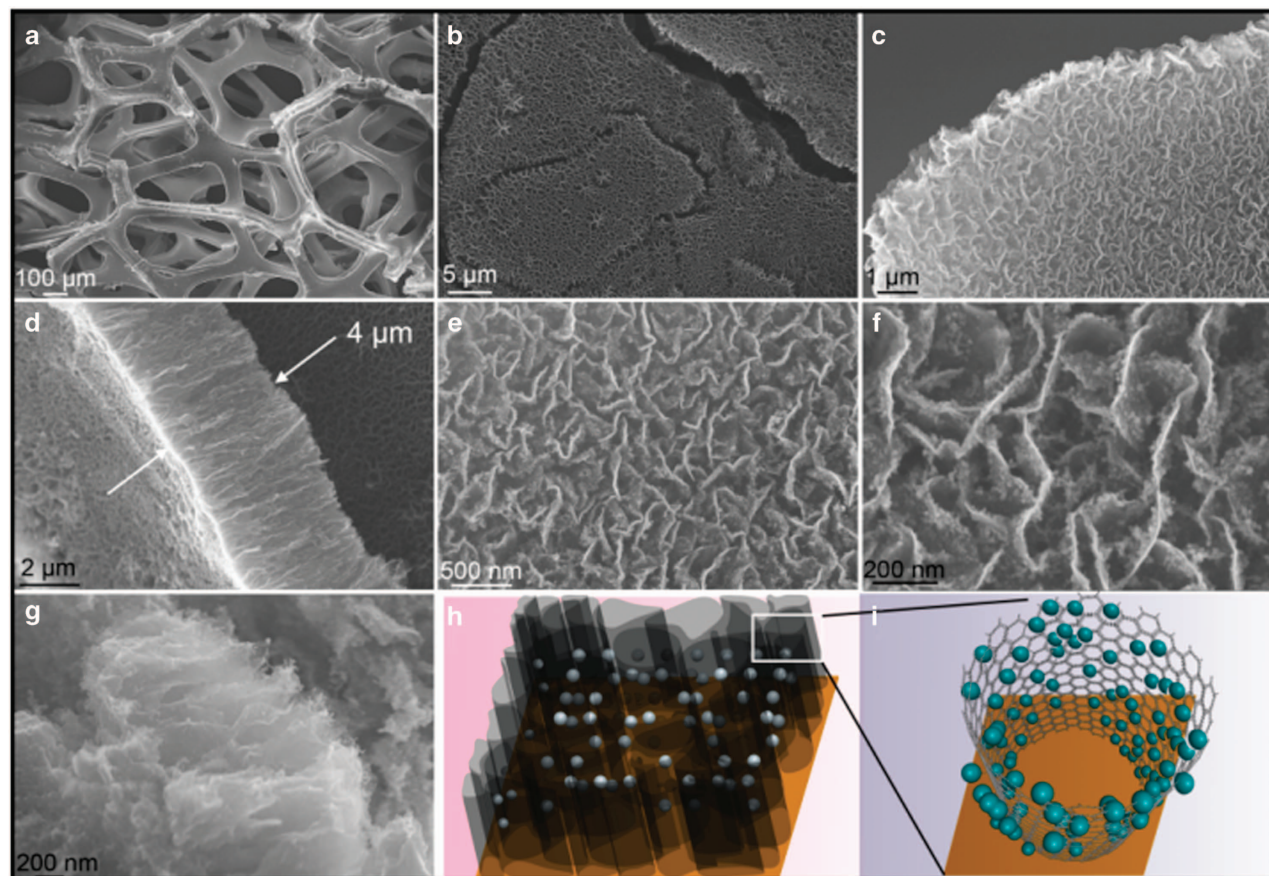


Figure 2 (a–c) Low magnification field emission scanning electron microscopy (FESEM) images of ruthenium (Ru)-decorated vertical graphene nanosheets (VGNS)@Ni foam. (d) Low magnification cross-sectional FESEM image of Ru@VGNS@Ni foam. (e–g) High magnification FESEM images of Ru@VGNS@Ni foam. (h, i) Schematic illustrations of the Ru-loaded VGNS@Ni foam.

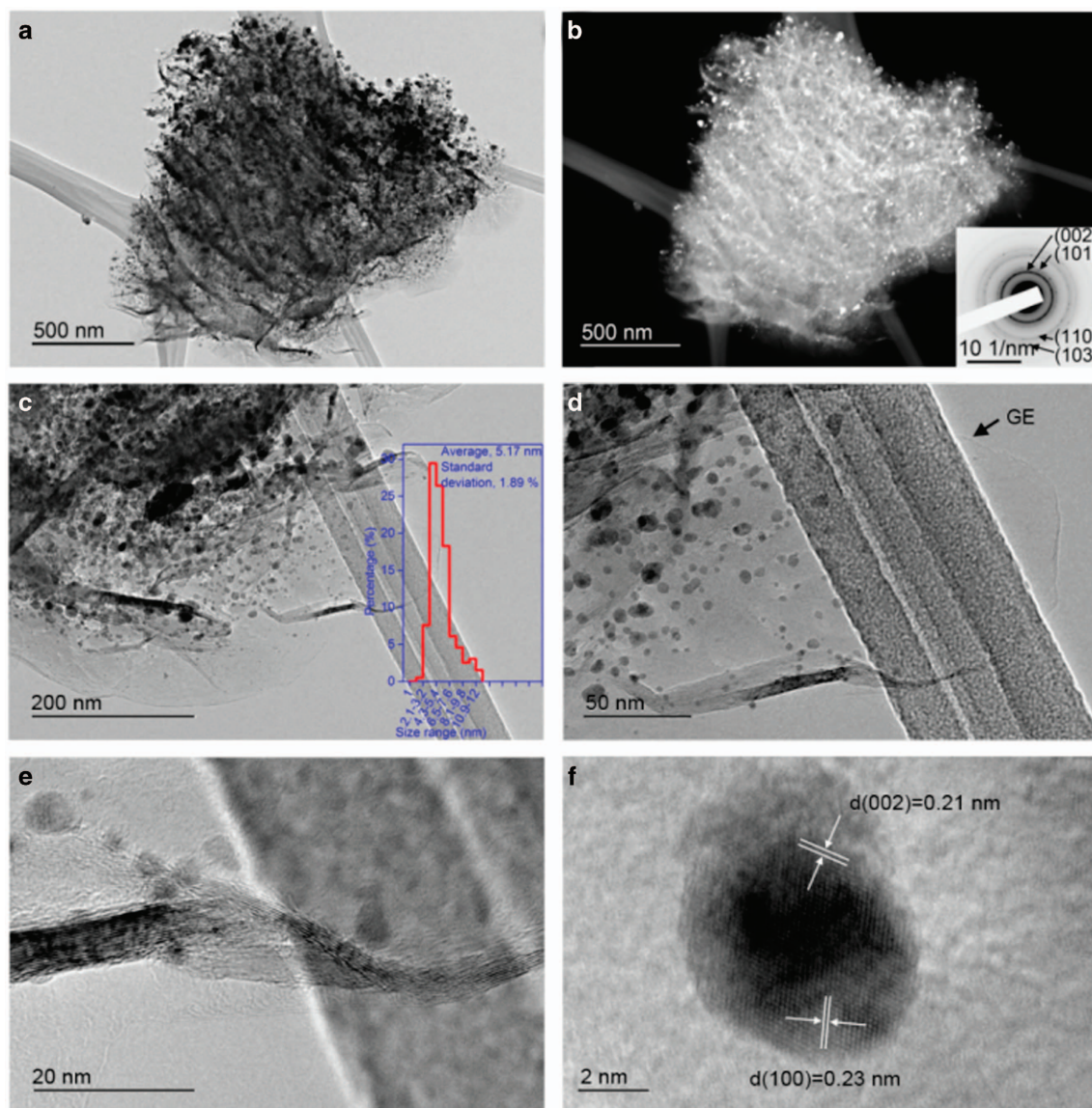


Figure 3 Transmission electron microscopy (TEM) images of ruthenium (Ru)-decorated vertical graphene nanosheets (VGNS)@Ni foam: (a) low magnification bright field TEM image; (b) corresponding low magnification dark field TEM image, with the inset showing the corresponding selected area electron diffraction (SAED) pattern; (c–e) high magnification TEM images; (f) lattice-resolved TEM image. Inset of (c) is the Ru nanocrystal size distribution.

The as-prepared Ru-decorated VGNS@Ni foam nanocomposite was characterized by TEM and HRTEM (Figure 3). Figure 3a shows a bright field TEM image of typical free-standing Ru-decorated VGNS, which exhibits the channels formed by the vertical graphene and the distribution of Ru nanoparticles. The corresponding dark field TEM image (Figure 3b) shows the uniform distribution of Ru nanoparticles on all of the vertical graphene sheets. The inset in Figure 3b is the corresponding selected area electron diffraction pattern of this free-standing Ru-decorated VGNS nanocomposite. The diffraction rings can be indexed to the (002), (101), (110) and (103) planes of hexagonal Ru crystals, indicating well-defined crystallinity. The average crystal size of Ru is 5.17 nm, calculated from the high magnification TEM image in Figure 3c. The HRTEM image in Figure 3d shows a free-standing graphene nanosheet, on which Ru nanoparticles are homogeneously distributed without aggregation. The average thickness of the VGNS is 3–4 atomic layers, as shown in the HRTEM image

(Figure 3e). The lattice-resolved HRTEM image further clearly shows that the Ru nanocrystals are uniformly anchored on the surfaces of the graphene nanosheets (Figure 3f). The crystal lattice can be indexed to the (100) and (002) crystal planes of Ru nanocrystals, with the d-spacings of 0.23 and 0.21 nm, respectively.

Electrochemical performance of VGNS@Ni foam and Ru-decorated VGNS@Ni foam in Li-O₂ cells

The electrocatalytic activities of VGNS@Ni foam and Ru-decorated VGNS@Ni foam were investigated. Galvanostatic charge–discharge measurements were carried out to evaluate the electrochemical performances in the voltage range of 2.0–4.3 V for VGNS@Ni foam and 2.0–4.2 V for Ru-decorated VGNS@Ni foam at room temperature. Typical charge–discharge voltage profiles are shown in Figure 4. It can be seen that VGNS@Ni foam featured a high initial discharge capacity of 14 461 mAh g⁻¹ at a current density of 200 mA g⁻¹

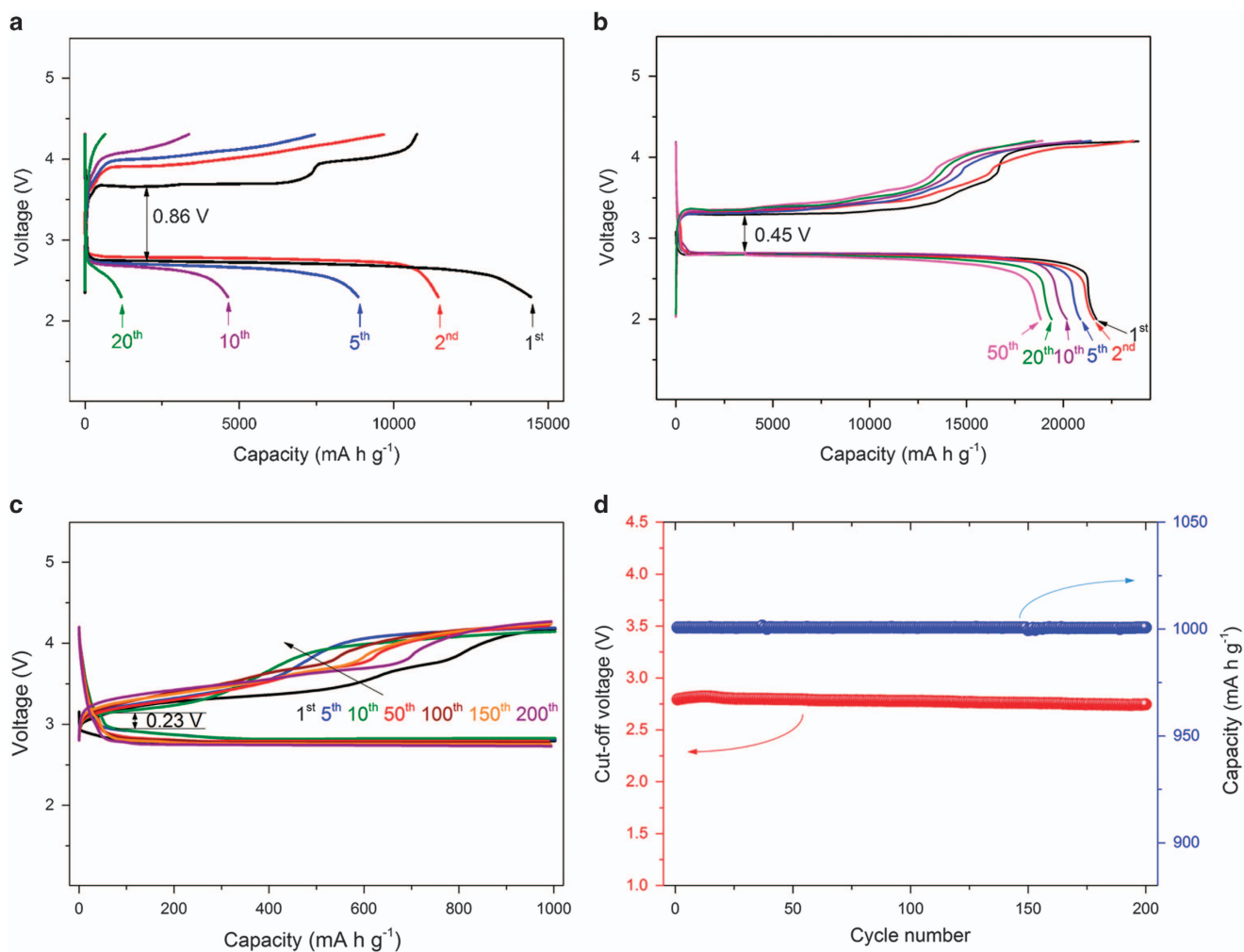


Figure 4 (a) Charge–discharge profiles of the bare vertical graphene nanosheets (VGNS)@Ni foam electrode at a current density of 200 mA g^{-1} . (b) Charge–discharge profiles of the ruthenium (Ru)-decorated VGNS@Ni foam electrode at a current density of 200 mA g^{-1} . (c) Charge–discharge profiles of Ru-decorated VGNS@Ni foam electrode with the capacity restricted to 1000 mA h g^{-1} at 200 mA g^{-1} current density. (d) Corresponding cycling performance with a fixed capacity of 1000 mA h g^{-1} at 200 mA g^{-1} current density.

(Figure 4a). The capacity is higher compared with those of other carbon-based cathode catalysts, indicating its superior electrochemical performance for Li-O₂ batteries.^{31–35} This should be ascribed to the unique 3D porous Ni foam network and the channel-structured vertical graphene.³¹ Furthermore, the channels enclosed by the vertical graphene provide active sites for storage of the reaction product, Li₂O₂, which contributes to the high discharge capacity. The reaction in the following charge process took place at the voltage of 3.65 V, which shows 0.86 V overpotential. The overpotential is significantly smaller than that of other carbon-based cathode materials for Li-O₂ batteries.^{36–39} The corresponding initial charge capacity is $10\,770 \text{ mA h g}^{-1}$ at the current density of 200 mA g^{-1} . Therefore, the charge capacity is lower than the discharge capacity, indicating that the Li₂O₂ product was not totally converted back to the Li⁺ and oxygen. In Figure 4a, there are two potential steps. The first one at $\sim 3.65 \text{ V}$ should be related to the decomposition of Li₂O₂. While the small plateau at $\sim 3.98 \text{ V}$ could be ascribed to the decomposition of by-products, such as lithium carboxylates (HCO₂Li and CH₃CO₂Li) and Li₂CO₃. As noted in the previous paper, these by-products were derived from electrolyte decomposition and the reaction between Li₂O₂ and carbon on discharge.^{40–42} The second discharge capacity

was $11\,455 \text{ mA h g}^{-1}$, and the corresponding charge capacity achieved was at 9701 mA h g^{-1} , indicating that irreversible reactions still occurred after the first cycle. Recently, it has been reported that by applying a trace amount of water in electrolytes, it can significantly reduce the charge overpotential and result in a small discharge–charge potential gap owing to the reversible formation and decomposition crystalline LiOH.^{43,44} The water content of the electrolyte was determined to be 34 p.p.m. with a Mettler Toledo C20 Karl Fischer Titrator. It was also reported that the charge potentials are dependent on the concentration of H₂O in electrolytes. In the dried dimethyl sulfoxide-based electrolyte, one charge potential plateau can be obtained at $\sim 3.65 \text{ V}$,⁴³ which is attributed to the oxidation of Li₂O₂ and in good agreement with the literatures.^{3,45} Based on our achieved charge potential at $\sim 3.65 \text{ V}$ of VGNS@Ni foam electrode, it indicates that the water does not involve in the reaction, consisted with the detected water concentration in the electrolyte. Owing to Li₂O₂ accumulated on the cathode side, the number of effective spaces for accommodating the Li₂O₂ generated from the following discharge processes will gradually decrease. As a result, the capacity continues degrading. The discharge capacity in the fifth cycle was 8880 mA h g^{-1} . After 20 cycles, only 1181 mA h g^{-1} discharge capacity was

maintained. Obviously, the irreversible ORR and OER reactions during the charge and discharge processes are the main reason for the decrease of the electrochemical performance. Therefore, it is important to identify suitable catalysts, which can improve the OER in the charge process for Li-O₂ batteries. Ru has been proven to be an effective catalyst for the OER of Li-O₂ batteries. Herein, we loaded Ru nanocrystals

on the VGNS@Ni foam. The charge and discharge profiles of the Ru-decorated VGNS@Ni foam are shown in Figure 4b. The initial discharge capacity reached up to 21 753 mAh g⁻¹, which is significantly higher than that of the bare VGNS@Ni foam electrode. Furthermore, the discharge plateau of Ru-decorated VGNS@Ni electrode is higher compared with that of the bare VGNS@Ni foam electrode (2.83 vs 2.73 V), indicating that the Ru nanocrystals have an enhanced catalytic activity towards the ORR. In the charge process, significant differences in the charge plateau were observed between the Ru-decorated VGNS@Ni foam electrode and the bare VGNS@Ni foam electrode (3.6 V for the bare VGNS@Ni foam electrode, and 3.2 V for the Ru-decorated VGNS@Ni foam electrode). The Ru-decorated VGNS@Ni foam electrode shows much lower charge plateaus compared with the bare VGNS@Ni foam electrode, demonstrating its excellent catalytic activity towards the OER. The overpotential between the charge and discharge processes has been significantly decreased by loading Ru nanocrystals. More importantly, an initial charge capacity of 23 864 mAh g⁻¹ was achieved, indicating that the reverse OER reaction of the Ru-decorated VGNS@Ni foam electrode was complete. As shown in Figure 4b, the charge curve is longer than that of discharge curve, which indicates the decomposition of electrolyte. The discharge capacity in the 2nd cycle was still 21 682 mAh g⁻¹, whereas the 5th, 10th and 20th cycle discharge capacities were 20 197, 20 920 and 19 435 mAh g⁻¹, respectively. Even after 50 cycles, the Ru-decorated VGNS@Ni foam electrode still achieved the high discharge capacity of 18 887 mAh g⁻¹. Moreover, the corresponding charge capacities were all maintained at a high level, indicating excellent cyclability. The overpotential between the charge and the discharge processes was maintained to be around 0.45 V for 50 cycles. The electrochemical performance is much better than the previously reported pure graphene electrode and Ru decorated carbon electrode.^{46,47}

The electrochemical performance of Ru-decorated VGNS@Ni foam electrode was further examined by restricting the capacity during cycling at various current densities. Figure 4c shows the voltage profiles of Ru-decorated VGNS@Ni foam electrode cycled at 200 mA g⁻¹, with the capacity restricted to 1000 mAh g⁻¹. The Ru-decorated VGNS@Ni foam electrode displays a discharge plateau at about 2.9 V. Furthermore, it also presents a low charge plateau, of 3.16 V. Comparing with the bare VGNS@Ni foam electrode, the Ru-decorated electrode shows a significantly decreased overpotential. The low charge potential (0.23 V) of the Ru-decorated VGNS@Ni foam electrode has been maintained for more than 200 cycles. From Figure 4d, it can be seen that there is no change on the cutoff voltage along the 200 cycles, confirming the outstanding cycling performance. We also tested the Ru-decorated VGNS@Ni foam electrode at different current densities, as shown in Supplementary Figure S3. When the current density was increased to 300 mA g⁻¹, a 0.35 V overpotential between the charge and discharge processes occurred and the low overpotential was sustained for more than 200 cycles (Supplementary Figure S3a). The same trend was also observed when the Ru-decorated VGNS@Ni foam electrodes were tested at current densities of 400 and 500 mA g⁻¹. The Li-O₂ cells achieved

low overpotential of 0.41 and 0.43 V, respectively. All of them can maintain cycling for more than 200 cycles (Supplementary Figures S3b and c). Even when the current density was increased to 800 mA g⁻¹, the Ru-decorated VGNS@Ni foam electrode still presented a very low charge plateau (Supplementary Figure S3d). These results indicate the high catalytic activity towards the OER of the Ru-decorated electrode.

To identify the charge and discharge products, we conducted *ex situ* XRD and s.e.m. measurements. As confirmed by the *ex situ* XRD pattern (Figure 5a) of the Ru-decorated VGNS@Ni foam electrode, the main discharge product is Li₂O₂ (JCPDS Card No. 09-0355), with hexagonal symmetry (space group: P6), apart from the Ru catalyst nanoparticles in the electrode. The morphologies of the Ru-decorated VGNS@Ni foam electrode in the fully discharged and charged states were analysed by *ex situ* FESEM (Figures 5b and c). As shown in Figure 5b, the Ru-decorated VGNS@Ni foam electrode was covered with the discharge product Li₂O₂ after being fully discharged. The Li₂O₂ has a toroid-like morphology with a particle size of about 500 nm, which is similar to the previously reported Li₂O₂ morphology.^{48,49} When the cell was fully charged, all the discharge products completely disappeared, as shown in Figure 5c. These results suggest that the Ru-decorated VGNS@Ni foam electrode can effectively catalyse the decomposition of Li₂O₂. To confirm the main discharge products after long cycling, the fully discharged Ru-decorated VGNS@Ni foam electrode was investigated after 20 cycles by *ex situ* Raman and Fourier transform infrared measurements. In the Raman spectrum (Figure 5d), two main Raman shifts at 1320 and 1600 cm⁻¹ correspond to the D- and G-band of carbon, respectively. The Raman shift at around 787 cm⁻¹ confirms the existence of Li₂O₂, as shown by the inset of Figure 5d. From the Fourier transform infrared spectrum (Supplementary Figure S4), the formation of Li₂O₂ can be further identified by the peaks at around 439 and 531 cm⁻¹. The peaks at ~870, 1420, 1500 and 1580 cm⁻¹ could be assigned to a mixture of Li₂CO₃ and HCO₂Li, as reported previously.¹ The spikes-shaped curves at around 1500 cm⁻¹ and the peak at 670 cm⁻¹ correspond to the background. The reactions during discharge and charge in the Li-O₂ cell are complex multiphase processes. It is considered that *in situ* analysis of discharge and charge processes is an effective method to identify the reaction mechanism. Therefore, we conducted the *in situ* DEMS to monitor the O₂ consumption and evolution during cell operation to confirm that the discharge-charge processes were overwhelmingly dominated by ORR/OER in Ru-decorated VGNS@Ni foam Li-O₂ cell. The Li-O₂ cell was first discharged under a flow of mixed gas of O₂/Ar. As shown in Figure 5e, O₂ consumption was measured for the Li-O₂ cells from the start of discharge process and continued along the increase of time. The DEMS results suggest that the discharge reactions are dominated by consumption of O₂ and formation of Li₂O₂. To understand the OER process (i.e. Li₂O₂ oxidation to O₂), the evolved gas during the charging process was also analysed. As shown in Figure 5f, it can be seen that O₂ evolution was detected from the beginning and continued along the voltage plateau of 3.2 V during most of the charging process. The cell voltage was maintained under 3.4 V until a decrease of O₂ evolution took place. There is no evolution of CO₂ during the whole charging process. It clearly demonstrates that Ru-decorated VGNS@Ni foam electrode can significantly reduce the charge overpotentials of OER in Li-O₂ cell and the specific charge capacity was mainly dominated by the evolution of O₂.

The Scheme 1 shows the catalytic mechanism for the Ru-decorated VGNS@Ni foam cathode in Li-O₂ batteries. The Ru-decorated VGNS@Ni foam cathode can provide sufficient pathways for the

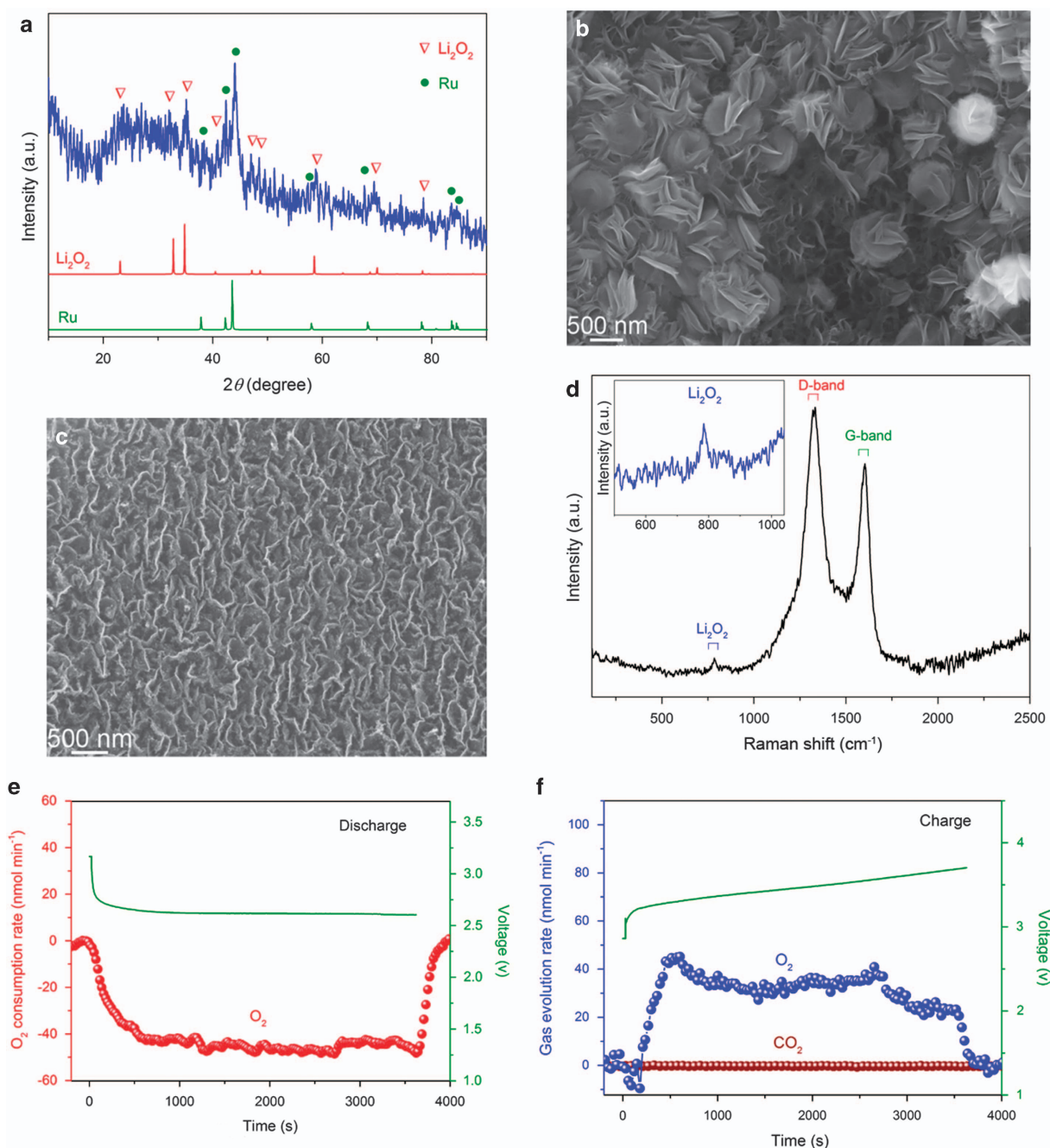
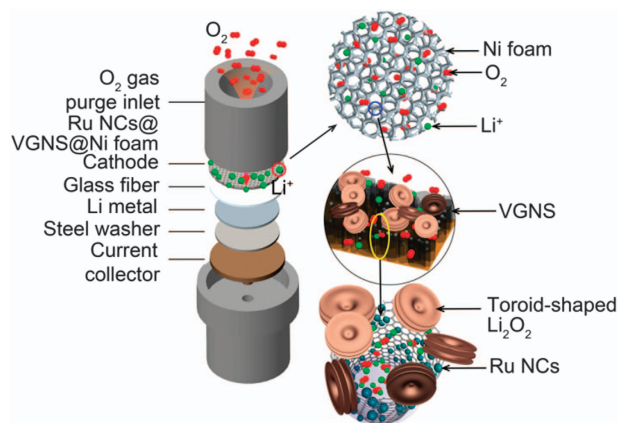


Figure 5 (a) *Ex situ* X-ray diffraction (XRD) pattern of discharged ruthenium (Ru)-decorated vertical graphene nanosheets (VGNS)@Ni foam electrode. (b, c) *Ex situ* field emission scanning electron microscopy (FESEM) images of Ru-decorated VGNS@Ni foam electrode: (b) in the fully discharged state and (c) in the fully charged state. (d) *Ex situ* Raman spectra of discharged Ru-decorated VGNS@Ni foam electrode. The inset is an enlargement of the Li_2O_2 peak. (e) *In situ* differential electrochemical mass spectrometry (DEMS) analysis of the O_2 consumption of Ru-decorated VGNS@Ni foam electrode during discharge process. (f) *In situ* DEMS analysis of O_2 and CO_2 evolution of Ru-decorated VGNS@Ni foam electrode during charge process.

diffusion of oxygen, owing to the 3D porous architecture of Ni foam skeleton. Furthermore, the VGNS on the Ni foam can facilitate the adsorption of oxygen molecules on the surface of graphene nanosheets because of the high surface area. As reported previously,^{48,50} O_2 is first bound to the cathode surface via oxygen vacancies, especially on the carbon defect sites and Ru catalyst nanoparticles, followed by reduction to O^{2-} . The stabilized superoxide ions could be combined via the dismutase reaction to form Li_2O_2 . This mechanism has been

confirmed by the presence of large (~ 500 nm) uniform toroid-shaped Li_2O_2 particles formed during the discharge process. In addition, the large toroid-shaped Li_2O_2 particles consist of aggregates of Li_2O_2 nanocrystals. This provides evidence for that the solvated LiO_2 is initially formed when the ORR catalysis reaches a local high saturation concentration. The Li_2O_2 nucleates to create nanocrystals because of its low solubility and is gradually deposited to form the observed 'tortellini' aggregate morphology. For the OER process on charge, it



Scheme 1 Schematic illustration for the catalytic reaction mechanism of the ruthenium (Ru)-decorated vertical graphene nanosheets (VGNS)@Ni foam as cathode in the Li-O₂ cell.

was proposed that lithium peroxide is decomposed into Li⁺ and O₂²⁻ on the vacant catalyst sites first, and then stepwisely oxidized to O²⁻ and O₂.^{48,50}

CONCLUSIONS

In summary, we report the synthesis of VGNS@Ni foam and Ru-decorated VGNS@Ni foam as an efficient cathode catalyst for Li-O₂ batteries. The electrochemical testing shows that the Ru-decorated VGNS@Ni foam is an effective cathode catalyst for Li-O₂ batteries, which can significantly reduce the charge overpotential and achieves a high specific capacity, leading to an enhanced electrochemical performance. In particular, the Ru-decorated VGNS@Ni foam demonstrated low charge overpotential (~0.45 V) and a high reversible capacity of about 23 864 mAh g⁻¹ at the current density of 200 mA g⁻¹. Ru-nanocrystal-decorated VGNS@Ni foam also demonstrated superior cycling stability at different current densities up to 200 cycles, with the capacity restricted to 1000 mAh g⁻¹. We also showed that Ru-decorated VGNS@Ni foam can effectively decompose the discharge product Li₂O₂, facilitate the OER and lead to high round-trip efficiency. The superior electrochemical performance of the Ru-decorated VGNS@Ni foam should be ascribed to the unique 3D porous Ni foam network and channel-structured VGNS. Furthermore, the channels enclosed by the vertical graphene provide spaces to accommodate the reaction product (Li₂O₂), contributing to the high discharge capacity. Therefore, Ru-decorated VGNS@Ni foam is a promising cathode catalyst for rechargeable Li-O₂ batteries with low charge overpotential, long cycle life and high specific capacity.

CONFLICT OF INTEREST

The authors declare no conflict of interest.

ACKNOWLEDGEMENTS

This original research was proudly supported by the Commonwealth of Australia through the Automotive Australia 2020 Cooperative Research Centre (AutoCRC) and ARC Future Fellowship Project (FT1101000800). This research was also financially supported by National Research Foundation (NRF) of Korea (No. 2016R1A2A1A05005344). The research used the TEM facility located at the UOW Electron Microscopy Centre, which was funded by an Australian Research Council (ARC) Linkage, Infrastructure, Equipment and Facilities (LIEF) grant (LE0237478). We thank Dr Tania Silver for critical reading.

- Peng, Z., Freunberger, S. A., Chen, Y. & Bruce, P. G. A reversible and higher-rate Li-O₂ battery. *Science* **337**, 563–566 (2012).
- Bruce, P. G., Freunberger, S. A., Hardwick, L. J. & Tarascon, J.-M. Li-O₂ and Li-S batteries with high energy storage. *Nat. Mater.* **11**, 19–29 (2012).
- Thotiyil, M. M. O., Freunberger, S. A., Peng, Z., Chen, Y., Liu, Z. & Bruce, P. G. A stable cathode for the aprotic Li-O₂ battery. *Nat. Mater.* **12**, 1050–1056 (2013).
- Li, F., Tang, D.-M., Chen, Y., Golberg, D., Kitaura, H., Zhang, T., Yamada, A & Zhou, H. Ru/ITO: a carbon-free cathode for nonaqueous Li-O₂ battery. *Nano Lett.* **13**, 4702–4707 (2013).
- Lu, J., Li, L., Park, J.-B., Sun, Y.-K., Wu, F. & Amine, K. Aprotic and aqueous Li-O₂ batteries. *Chem. Rev.* **114**, 5611–5640 (2014).
- Zhao, G., Mo, R., Wang, B., Zhang, L. & Sun, K. Enhanced cyclability of Li-O₂ batteries based on TiO₂ supported cathodes with no carbon or binder. *Chem. Mater.* **26**, 2551–2556 (2014).
- Han, X., Cheng, F., Chen, C., Hu, Y. & Chen, J. Uniform MnO₂ nanostructures supported on hierarchically porous carbon as efficient electrocatalysts for rechargeable Li-O₂ batteries. *Nano Res.* **8**, 154–164 (2015).
- Li, Q., Xu, P., Gao, W., Ma, S., Zhang, G., Cao, R., Wang, H. L. & Wu, G. Graphene/graphene-tube nanocomposites templated from cage-containing metal-organic frameworks for oxygen reduction in Li-O₂ batteries. *Adv. Mater.* **26**, 1378–1386 (2014).
- Zhang, J., Li, P., Wang, Z., Qiao, J., Rooney, D., Sun, W. & Sun, K. Three-dimensional graphene-Co₃O₄ cathodes for rechargeable Li-O₂ batteries. *J. Mater. Chem. A* **3**, 1504–1510 (2015).
- Park, J., Jun, Y.-S., Lee, W.-R., Gerbec, J. A., See, K. A. & Stucky, G. D. Bimodal mesoporous titanium nitride/carbon microfibers as efficient and stable electrocatalysts for Li-O₂ batteries. *Chem. Mater.* **25**, 3779–3781 (2013).
- Xiao, D., Dong, S., Guan, J., Gu, L., Li, S., Zhao, N., Shang, C., Yang, Z., Zheng, H., Chen, C. & Xiao, R. Direct observation of ordered oxygen defects on the atomic scale in Li₂O₂ for Li-O₂ batteries. *Adv. Energy Mater.* **14**, 1400664 (2015).
- Lau, K. C., Lu, J., Low, J., Peng, D., Wu, H., Albishri, H. M., Al-Hady, D. A., Curtiss, L. A. & Amine, K. Investigation of the decomposition mechanism of lithium bis (oxalate) borate (LiBOB) salt in the electrolyte of an aprotic Li-O₂ battery. *Energy Technol.* **2**, 348–354 (2014).
- Monaco, S., Soavi, F. & Mastragostino, M. Role of oxygen mass transport in rechargeable Li/O₂ batteries operating with ionic liquids. *J. Phys. Chem. Lett.* **4**, 1379–1382 (2013).
- Horstmann, B., Gallant, B., Mitchell, R., Bessler, W. G., Shao-Horn, Y. & Bazant, M. Z. Rate-dependent morphology of Li₂O₂ growth in Li-O₂ batteries. *J. Phys. Chem. Lett.* **4**, 4217–4222 (2013).
- Kang, S., Mo, Y., Ong, S. P. & Ceder, G. A facile mechanism for recharging Li₂O₂ in Li-O₂ batteries. *Chem. Mater.* **25**, 3328–3336 (2013).
- Das, U., Lau, K. C., Redfern, P. C. & Curtiss, L. A. Structure and stability of lithium superoxide clusters and relevance to Li-O₂ batteries. *J. Phys. Chem. Lett.* **5**, 813–819 (2014).
- Xu, J. J., Xu, D., Wang, Z. L., Wang, H. G., Zhang, L. L. & Zhang, X. B. Synthesis of perovskite-based porous La_{0.75}Sr_{0.25}MnO₃ nanotubes as a highly efficient electrocatalyst for rechargeable lithium-oxygen batteries. *Angew. Chem. Int. Ed.* **52**, 3887–3890 (2013).
- Li, C., Zhang, W., Ang, H. X., Yu, H., Wang, X., Hng, H. H. & Yan, Q. Y. Compressed hydrogen gas-induced synthesis of Au-Pt core/shell nanoparticle chains towards high-performance catalysts for Li-O₂ batteries. *J. Mater. Chem. A* **2**, 10676–10681 (2014).
- Dong, S., Wang, S., Guan, J., Li, S., Lan, Z., Chen, C., Shang, C., Zhang, L., Wang, X., Gu, L., Cui, G. & Chen, L. Insight into enhanced cycling performance of Li-O₂ batteries based on binary CoSe₂/CoO nanocomposite electrodes. *J. Phys. Chem. Lett.* **5**, 615–621 (2014).
- Bryantsev, V. S., Giordani, V., Walker, W., Uddin, J., Lee, I., van Duin, A. C., Chase, G. V. & Addison, D. Investigation of fluorinated amides for solid-electrolyte interphase stabilization in Li-O₂ batteries using amide-based electrolytes. *J. Phys. Chem. C* **117**, 11977–11988 (2013).
- Yilmaz, E., Yogi, C., Yamanaka, K., Ohta, T. & Byon, H. R. Promoting formation of noncrystalline Li₂O₂ in the Li-O₂ battery with RuO₂ nanoparticles. *Nano Lett.* **13**, 4679–4684 (2013).
- Jian, Z., Liu, P., Li, F., He, P., Guo, X., Chen, M. & Zhou, H. Core-shell-structured CNT@RuO₂ composite as a high-performance cathode catalyst for rechargeable Li-O₂ batteries. *Angew. Chem. Int. Ed.* **53**, 442–446 (2014).
- Bhattacharya, P., Nasybulin, E. N., Engelhard, M. H., Kovarik, L., Bowden, M. E., Li, X. S., Gaspar, D. J., Xu, W. & Zhang, J. G. Dendrimer-encapsulated ruthenium oxide nanoparticles as catalysts in lithium-oxygen batteries. *Adv. Funct. Mater.* **24**, 7510–7519 (2014).
- Miller, J. R., Outlaw, R. & Holloway, B. Graphene double-layer capacitor with ac line-filtering performance. *Science* **329**, 1637–1639 (2010).
- Chen, J., Sheng, K., Luo, P., Li, C. & Shi, G. Graphene hydrogels deposited in nickel foams for high-rate electrochemical capacitors. *Adv. Mater.* **24**, 4569–4573 (2012).
- Yan, Z., Ma, L., Zhu, Y., Lahiri, I., Hahm, M. G., Liu, Z., Yang, S., Xiang, C., Lu, W., Peng, Z., Sun, Z., Kittrell, C., Lou, J., Choi, W., Ajayan, P. M. & Tour, J. M. Three-dimensional metal-graphene-nanotube multifunctional hybrid materials. *ACS Nano* **7**, 58–64 (2012).
- Obraztsov, A. N. Chemical vapour deposition: making graphene on a large scale. *Nat. Nano* **4**, 212–213 (2009).
- Ostrikov, K. Colloquium: reactive plasmas as a versatile nanofabrication tool. *Rev. Mod. Phys.* **77**, 489 (2005).

- 29 Sun, B., Munroe, P. & Wang, G. Ruthenium nanocrystals as cathode catalysts for lithium-oxygen batteries with a superior performance. *Sci. Rep.* **3**, 2247 (2013).
- 30 Yang, P., Zhao, D., Margolese, D. I., Chmelka, B. F. & Stucky, G. D. Generalized syntheses of large-pore mesoporous metal oxides with semicrystalline frameworks. *Nature* **396**, 152–155 (1998).
- 31 Wang, Z.-L., Xu, D., Xu, J.-J., Zhang, L.-L. & Zhang, X.-B. Graphene oxide gel-derived, free-standing, hierarchically porous carbon for high-capacity and high-rate rechargeable Li-O₂ batteries. *Adv. Funct. Mater.* **22**, 3699–3705 (2012).
- 32 Mitchell, R. R., Gallant, B. M., Thompson, C. V. & Shao-Horn, Y. All-carbon-nanofiber electrodes for high-energy rechargeable Li-O₂ batteries. *Energy Environ. Sci.* **4**, 2952–2958 (2011).
- 33 Zhang, T. & Zhou, H. From Li-O₂ to Li-air batteries: carbon nanotubes/ionic liquid gels with a tricontinuous passage of electrons, ions, and oxygen. *Angew. Chem. Int. Ed.* **51**, 11062–11067 (2012).
- 34 Shui, J., Du, F., Xue, C., Li, Q. & Dai, L. Vertically aligned N-doped coral-like carbon fiber arrays as efficient air electrodes for high-performance nonaqueous Li-O₂ batteries. *ACS Nano* **8**, 3015–3022 (2014).
- 35 Guo, Z., Zhou, D., Dong, X., Qiu, Z., Wang, Y. & Xia, Y. Ordered hierarchical mesoporous/macroporous carbon: a high-performance catalyst for rechargeable Li-O₂ batteries. *Adv. Mater.* **25**, 5668–5672 (2013).
- 36 Ding, N., Chien, S. W., Hor, T. S. A., Lum, R., Zong, Y. & Liu, Z. Influence of carbon pore size on the discharge capacity of Li-O₂ batteries. *J. Mater. Chem. A* **2**, 12433–12441 (2014).
- 37 Lim, H. D., Park, K. Y., Song, H., Jang, E. Y., Gwon, H., Kim, J., Kim, Y. H., Lima, M. D., Ovalle Robles, R., Lepró, X., Baughman, R. H. & Kang, K. Enhanced power and rechargeability of a Li-O₂ battery based on a hierarchical-fibril CNT electrode. *Adv. Mater.* **25**, 1348–1352 (2013).
- 38 Chen, Y., Li, F., Tang, D.-M., Jian, Z., Liu, C., Golberg, D., Yamada, A. & Zhou, H. Multi-walled carbon nanotube papers as binder-free cathodes for large capacity and reversible non-aqueous Li-O₂ batteries. *J. Mater. Chem. A* **1**, 13076–13081 (2013).
- 39 Park, J.-B., Lee, J., Yoon, C. S. & Sun, Y.-K. Ordered mesoporous carbon electrodes for Li-O₂ batteries. *ACS Appl. Mater. Inter.* **5**, 13426–13431 (2013).
- 40 Jiang, J., He, P., Tong, S. F., Zheng, M. B., Lin, Z. X., Zhang, X. P., Shi, Y. & Zhou, H. S. Ruthenium functionalized graphene aerogels with hierarchical and three-dimensional porosity as a free-standing cathode for rechargeable lithium-oxygen batteries. *NPG Asia Mater.* **8**, e239 (2016).
- 41 Ottakam Thotiyl, M. M., Freunberger, S. A., Peng, Z. & Bruce, P. G. The carbon electrode in nonaqueous Li-O₂ cells. *J. Am. Chem. Soc.* **135**, 494–500 (2012).
- 42 Freunberger, S. A., Chen, Y., Drewett, N. E., Hardwick, L. J., Bardé, F. & Bruce, P. G. The lithium-oxygen battery with ether-based electrolytes. *Angew. Chem. Int. Ed.* **50**, 8609–8613 (2011).
- 43 Li, F., Wu, S., Zhang, T., He, P., Yamada, A. & Zhou, H. The water catalysis at oxygen cathodes of lithium-oxygen cells. *Nat. Commun.* **6**, 7843 (2015).
- 44 Liu, T., Leskes, M., Yu, W., Moore, A. J., Zhou, L., Bayley, P. M., Kim, G. & Grey, C. P. Cycling Li-O₂ batteries via LiOH formation and decomposition. *Science* **350**, 530–533 (2015).
- 45 Li, F., Tang, D. M., Jian, Z., Liu, D., Golberg, D., Yamada, A. & Zhou, H. Li-O₂ battery based on highly efficient Sb-doped tin oxide supported Ru nanoparticles. *Adv. Mater.* **26**, 4659–4664 (2014).
- 46 Sun, B., Wang, B., Su, D., Xiao, L., Ahn, H. & Wang, G. Graphene nanosheets as cathode catalysts for lithium-air batteries with an enhanced electrochemical performance. *Carbon* **50**, 727–733 (2012).
- 47 Jung, H.-G., Jeong, Y. S., Park, J.-B., Sun, Y.-K., Scrosati, B. & Lee, Y. J. Ruthenium-based electrocatalysts supported on reduced graphene oxide for lithium-air batteries. *ACS Nano* **7**, 3532–3539 (2013).
- 48 Oh, S. H., Black, R., Pomerantseva, E., Lee, J.-H. & Nazar, L. F. Synthesis of a metallic mesoporous pyrochlore as a catalyst for lithium-O₂ batteries. *Nat. Chem* **4**, 1004–1010 (2012).
- 49 Xu, J.-J., Wang, Z.-L., Xu, D., Zhang, L.-L. & Zhang, X.-B. Tailoring deposition and morphology of discharge products towards high-rate and long-life lithium-oxygen batteries. *Nat. Commun.* **4**, 2438 (2013).
- 50 Laoire, C. O., Mukerjee, S., Abraham, K., Plichta, E. J. & Hendrickson, M. A. Elucidating the mechanism of oxygen reduction for lithium-air battery applications. *J. Phys. Chem. C* **113**, 20127–20134 (2009).



This work is licensed under a Creative Commons Attribution 4.0 International License. The images or other third party material in this article are included in the article's Creative Commons license, unless indicated otherwise in the credit line; if the material is not included under the Creative Commons license, users will need to obtain permission from the license holder to reproduce the material. To view a copy of this license, visit <http://creativecommons.org/licenses/by/4.0/>

© The Author(s) 2016

Supplementary Information accompanies the paper on the NPG Asia Materials website (<http://www.nature.com/am>)